THE AMERICAN SOCIETY OF MECHANICAL ENGINEERS
345 E. 47th St., New York, N.Y. 10017

97-GT-405

A SHOCK LOSS MODEL FOR SUPERSONIC COMPRESSOR CASCADES

Gregory S. Bloch
William W. Copenhaver
Aero Propulsion and Power Directorate
Wright Laboratory
Wright-Patterson AFB, OH

Walter F. O'Brien
Mechanical Engineering Department
Virginia Polytechnic Institute and State University
Blacksburg, VA

Abstract

Loss models used in compression system performance prediction codes are often developed from the study of two-dimensional cascades. In this paper, compressible fluid mechanics has been applied to the changes in shock geometry that are known to occur with back pressure for unstarted operation of supersonic compressor cascades. This physics-based engineering shock loss model is applicable to cascades with arbitrary airfoil shapes.

Predictions from the present method have been compared to measurements and Navier-Stokes analyses of the L030-4 and L030-6 cascades, and very good agreement was demonstrated for unstarted operation. A clear improvement has been demonstrated over previously published shock loss models for unstarted operation, both in the accuracy of the predictions and in the range of applicability.

The dramatic increase in overall loss with increasing inlet flow angle is shown to be primarily the result of increased shock loss, and much of this increase is caused by the detached bow shock. For a given Mach number, the viscous profile loss is nearly constant over the entire unstarted operating range of the cascade, unless a shock-induced boundary layer separation occurs near stall. Shock loss is much more sensitive to inlet Mach number than is viscous profile loss.

Nomenclature

A	relative flow area
$AVDR$	axial velocity density ratio
c	blade chord
c_p	specific heat at constant pressure
F	compressible mass flow function
h	blade or streamtube height
LER	leading edge radius
$\dot{m}$	mass flow rate
M	Mach number
P	pressure
s	tangential blade spacing
t	blade thickness
T	temperature

Greek Symbols

β	relative flow angle
γ	ratio of specific heats
ν	Prandtl-Meyer function
μ	Mach angle, $\sin^{-1}(1/M)$
ω	total pressure loss coefficient, $\omega = \frac{P_{01} - P_0}{P_{01} - P_1}$

Subscripts

A	conditions along first captured Mach wave
x	axial component
0	total property
1	conditions at upstream location
2	conditions at downstream location

Embellishments

$\bar{}$	averaged property

Introduction

The detailed design of transonic compressors is typically performed using a streamline curvature method of solution of the equations of fluid motion. The flow is assumed to be axisymmetric, and the effects of entropy generation are included as total pressure losses determined from loss models (e.g., Lieblein, 1954; Novak, 1967). These methods can be used either as analytical tools to predict the flow field from a known geometry, or in an inverse mode to predict the blade shape needed to generate a desired flow.

It has been suggested that the use of streamline curvature methods should be abandoned in favor of Navier-Stokes codes (e.g., Denton, 1994). While a direct numerical solution of the Navier-Stokes equations can yield a very detailed qualitative description of the flow field for a known geometry, there are still several limitations to the use of CFD in the design process. Navier-Stokes methods are quite expensive in terms of computer resources and time required for solution, and are currently unable to predict losses accurately. The inability to accurately quantify loss is a direct result of a poor

Presented at the International Gas Turbine & Aeroengine Congress & Exhibition
Orlando, Florida — June 2–June 5, 1997
This paper has been accepted for publication in the Transactions of the ASME
Discussion of it will be accepted at ASME Headquarters until September 30, 1997

fundamental understanding of turbulence and boundary layer transition, and this situation is not expected to improve in the near future (Casey, 1994b; Denton, 1993; Vuillez and Petot, 1994; Jennions, 1994). Also, such methods are not presently used in an inverse mode to provide the blade shape required to generate a desired flow field. In spite of these disadvantages, CFD is used extensively to obtain designs which operate closer to the physical separation and choking limits of the machine, and to reduce development time, expense, and risk. However, these CFD optimizations are performed on preliminary designs that are obtained by streamline curvature methods.

It is generally accepted that streamline curvature methods will provide a satisfactory prediction of compressor performance as long as the losses, blockage, and deviation are predicted accurately. As a result, it is expected that the use of these tools in the design process will continue for many years. It follows that there is wide agreement on the need for improvements in loss modeling to support the streamline curvature tools (Koch, 1995; Dunham, 1995; Casey, 1994a).

Miller, et al. (1961) assumed that a normal shock extended from the blade leading edge to the suction surface, normal to the mean passage camber line, and calculated the loss from a single shock with a representative upstream Mach number. Wennerstrom and Puterbaugh (1984) also assumed a normal passage shock in the cascade plane, but included the spanwise sweep of the shock that results from the increase in stagger angle from hub to tip, and performed a 3-point integration of the shock loss. Koch and Smith (1976) assumed that the passage shock generates the entropy rise equivalent to 1 oblique shock that reduces a representative passage inlet Mach number to unity, and included an empirical correlation to account for the leading edge bluntness.

The application of the above models is restricted to design-point operation because they do not address the changes in shock geometry that occur with changes in back pressure. Calculation of off-design shock losses requires an accurate *a priori* knowledge of the shock geometry and Mach number (Balzer, 1971) or of flow angle significantly downstream of the shock (Freeman and Cumpsty, 1992), which limits the usefulness of these methods as predictive tools.

It would be desirable to have the ability to generate the entire compressor map from first principles so that a design could be optimized for maximum part-speed efficiency. This is where most man-rated engines spend the majority of their operating lives and this is where the largest benefit to the customer will be obtained. To realize this objective, the compressor designer must have the capability to perform accurate performance calculations over a range of back pressures and rotor speeds, and these calculations must be faster and cheaper than is currently possible with CFD codes.

This paper presents the application of compressible fluid mechanics to the changes in shock geometry that are known to occur with back pressure for unstarted operation of supersonic compressor cascades. This physics-based engineering shock loss model is applicable to cascades with arbitrary airfoil shapes.

Table 1. Geometric and design-point aerodynamic parameters for L030 rotor and cascades

	L030-4 45% span	L030-6 68% span
stagger	48.51°	55.71°
s/c	0.621	0.678
t/c	0.05	0.04
LER/s	0.004035	0.003168
M_1	1.0913	1.2237
M_2	0.7167	0.8110
β_1	58.66°	61.95°
β_2	46.17°	54.03°
P_2/P_1	1.464	1.517

Background

To assess the accuracy of the proposed shock loss model, the aero performance data from the L030-4 and L030-6 cascades are considered. These blade sections, which were tested at the DFVLR (now DLR), are the 45% span and 68% span of the L030 transonic research compressor rotor reported by Dunker, et al. (1978) and Dunker and Hungenberg (1980). The major blade geometric parameters and design-point aerodynamic parameters for these cascades are listed in Table 1, and details of the cascade experiment are given by Schreiber (1980, 1981) and by Schreiber and Starken (1981).

The overall total pressure loss coefficients presented for this experiment were obtained by momentum-averaging the exit-plane measurements. The fractions of the overall loss that are the result of the viscous blade boundary layer and the passage shock system were approximated by area-averaging the local total pressure loss coefficient (Schreiber, 1987; Schreiber and Tweedt, 1987). The edges of the viscous wake region were determined from traverse measurements, as shown in Figure 1, and the profile loss is given by

$$\omega_{profile} = \frac{1}{s}\int_{y_{ps}}^{y_{ss}} \omega dy - \frac{1}{s}\left(\frac{\omega_{y_{ps}} + \omega_{y_{ss}}}{2}\right)\left(y_{ss} - y_{ps}\right) \qquad (1)$$

The shock loss was then calculated as the difference between the "mixed-out" overall loss and the approximated value of profile loss.

$$\omega_{shock} = \overline{\omega} - \omega_{profile} \qquad (2)$$

Shock loss measurements from the aforementioned experiment were presented at discrete inlet flow angles by Schreiber (1987). Two flow angles were presented for the L030-6 cascade, and 3 flow angles for the L030-4 cascade. A typical curve is shown in Figure 2.

In an effort to improve the understanding of the qualitative variation of shock loss between the known measurements, Navier-Stokes analyses of the L030-4 and L030-6 cascades have been conducted. These analyses used the RVCQ3D (Rotor Viscous Code Quasi-3-D) solver developed for the analysis of blade-to-blade flows in turbomachinery (Chima, 1987; Chima, et al., 1987). Because viscous grids are typically much finer normal to the blade than in the streamwise direction, all viscous derivatives in the streamwise direction are dropped for lack of resolution (the "thin shear layer" approximation).

The RVCQ3D code uses a body-fitted C-type grid which is typically generated using a version of the GRAPE code developed by Sorenson

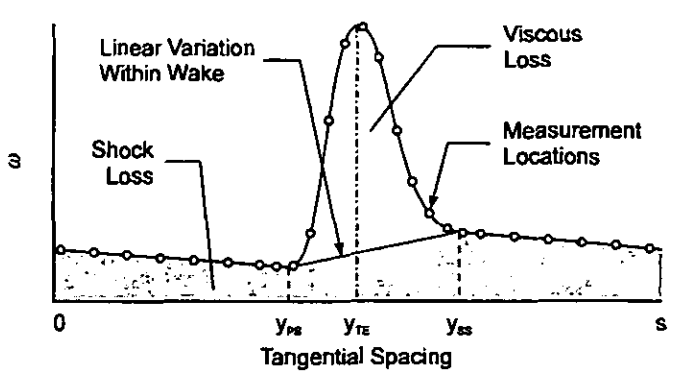

Figure 1. Shock and viscous losses in the measuring plane downstream of supersonic cascade

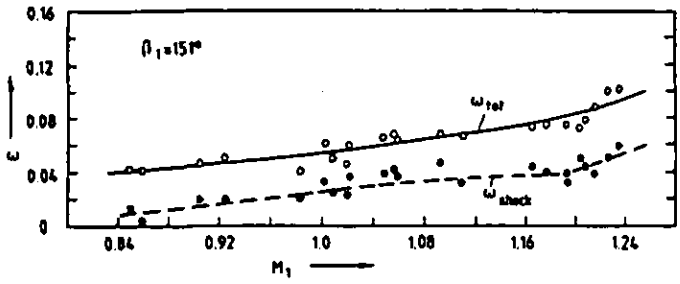

Figure 2. Influence of inlet Mach number on measured total pressure losses and corresponding shock losses of the L030-6 cascade (Schreiber, 1987)

(1981). An explicit 4-stage Runge-Kutta integration scheme was used to march forward in time from an initial guess to a steady-state solution (the number of integration stages is user-specified). A spatially-varying time step and implicit residual smoothing were used to accelerate convergence, and the Baldwin-Lomax turbulence model was used. The code uses a fourth difference artificial dissipation term to prevent odd-even decoupling and a second difference artificial dissipation term for shock capturing. The method is generally second order accurate, although it reduces to first order near shocks.

For the present investigation, a 321x70 grid was used to obtain solutions for both the L030-4 and the L030-6 cascades. Although streamtube contraction is known to have a significant impact on cascade performance, the exit static pressure and the AVDR are strongly coupled and only limited independent variations are possible in the cascade tests. The typical experimental procedure is to set the inlet Mach number and exit static pressure as close as possible to the desired values, and then measure the AVDR obtained from these settings (Schreiber and Tweedt, 1987). Because the streamtube contraction is not measured within the blade passage, and because AVDR information was not published by Schreiber (1987), the CFD solutions were obtained with no streamtube contraction ($AVDR = 1.0$).

An Engineering Shock Loss Model

The scope of the present model is restricted to the total pressure loss produced by the passage shock system that exists during unstarted operation of a 2-dimensional supersonic compressor cascade with arbitrary airfoil shapes. It is recognized that viscous effects related to the blade boundary layer and any shock-boundary layer interactions can have a significant impact on performance, but these effects must be addressed separately. Many treatises on the calculation of the minimum-incidence operating condition exist in the literature (e.g., Kantrowitz, 1950; Levine, 1956; Starken, 1971; Lichtfuß and Starken, 1974) so it will be treated briefly here. This is commonly referred to as the "unique incidence" condition, and these are the inlet conditions that exist at the cascade start/unstart point.

Consider an infinite cascade operating with an inlet flow that is supersonic relative to the blade but has an axial component that is subsonic, as shown in Figure 3. The flow upstream of the passage shock is assumed to be steady and inviscid. The present investigation is restricted to stationary cascades, so the total temperature is constant everywhere. Because the axial component of the flow is subsonic, the Mach waves emanating from the suction surface move upstream of the blade, allowing the cascade to influence the upstream flow. The curvature of the left-running characteristics caused by the detached bow shock is neglected in the present analysis, although the total pressure loss from the bow shock is included in the continuity equation in an approximate way, as suggested by Starken, et al. (1984).

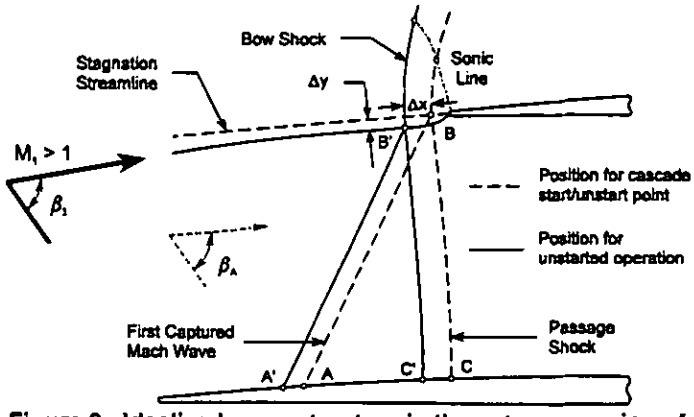

Figure 3. Idealized wave structure in the entrance region of a supersonic compressor cascade

As the flow passes around the leading edge, it will undergo a Prandtl-Meyer expansion from the upstream flow angle to be aligned with the blade suction surface. The first captured Mach wave extends from point A to the point where the stagnation streamline intersects the bow shock at point B. The flow region extending upstream from the first captured Mach wave is generally referred to as the "inlet region" or the "entrance region" of the cascade. The location of point A depends on suction surface curvature and upstream Mach number, and is determined by iteratively solving the Prandtl-Meyer and continuity relations. The Prandtl-Meyer relation is given by

$$\beta_1 + \nu(M_1) = \beta_A + \nu(M_A) \tag{3}$$

where ν is the well-known Prandtl-Meyer function.

$$\nu(M) = \sqrt{\left(\frac{\gamma+1}{\gamma-1}\right)}\tan^{-1}\sqrt{\left(\frac{\gamma-1}{\gamma+1}\right)\left(M^2-1\right)} - \tan^{-1}\sqrt{M^2-1} \tag{4}$$

The continuity relation is given by

$$\dot{m} = \frac{F(M_1)P_{01}s\cos\beta_1}{\sqrt{c_p T_{01}}} = \frac{F(M_A)P_{0A}\overline{AB}\sin\mu_A}{\sqrt{c_p T_{0A}}} \tag{5}$$

where F is the following compressible mass flow function.

$$F(M) = \frac{\dot{m}\sqrt{c_p T_0}}{P_0 A} = \frac{\gamma}{\sqrt{\gamma-1}} M\left\{1+\frac{\gamma-1}{2}M^2\right\}^{-\frac{\gamma+1}{2(\gamma-1)}} \tag{6}$$

In general, supersonic compressor blading has some finite leading edge radius for damage tolerance and this causes the bow shock to be slightly detached from the leading edge. The shape of this detached bow shock is approximated as a hyperbola that is normal to the flow directly ahead of the blade and asymptotically approaches the free-stream Mach lines, as suggested by Moeckel (1949). The vertex of this hyperbola is located at the vertex of a wedge, with half-angle 1° larger than the half-angle corresponding to shock detachment, placed tangent to the blunt leading edge as shown in Figure 4. The shape of the bow shock defined in this manner is uniquely determined by the upstream Mach number and the blade leading edge radius.

The Mach number immediately upstream of the bow shock will not be completely uniform because of the (generally) nonzero suction surface curvature and the deceleration produced by the infinite number of upstream bow waves. These variations are expected to be small, however, and the bow shock is treated as though it were in a uniform stream. The total pressure loss from the bow shock is then estimated by

numerically integrating the loss from a single wave between the stagnation streamline, point B, and infinity (Klapproth, 1950).

$$\frac{P_{0A}}{P_{01}} = 1 - \frac{\int_0^{\infty} \left(1 - \frac{P_{02}}{P_{01}}\right) dy}{\int_0^{s} dy} \tag{7}$$

where P_{02}/P_{01} is obtained from oblique shock theory.

If the back pressure is increased enough to unchoke the cascade, the passage shock will detach and move upstream of the blade leading edge by an amount Δx, as shown by the solid lines in Figure 3. As the passage shock moves upstream, the stagnation streamline will shift toward the suction surface of the lower adjacent blade by an amount Δy to provide the typical path for subsonic flow approaching an airfoil. (Point B' is located by extending a line upstream from point B by an amount Δx at an angle β_A relative to the axial direction and translating normal to this line, toward the suction surface, by an amount Δy.) These 2 effects cause the first captured Mach wave to move upstream and to become shorter. Because Equations 3 and 5 must always be satisfied, Δx and Δy are the primary mechanisms which allow the upstream flow angle to increase above the minimum value. Operation with a detached passage shock is commonly referred to as an "unstarted" cascade.

The relation between Δx and Δy for unstarted operation is not currently described by theory. To gain some understanding of this variation, the stagnation streamline was plotted from the unstarted CFD solutions generated for the L030-6 cascade with inlet Mach numbers of 1.100 and 1.200. The variation of Δx and Δy between choking and stall was then scaled from these stagnation streamlines for each Mach number, and was adequately described by the following relation.

$$\Delta x = 6\Delta y \tag{8}$$

To be clear, it is not suggested that the above relation will be exactly correct for all blade profiles. Although the relation between Δx and Δy was similar for both of the above cases, it is anticipated that this relation will be slightly different for every blade shape and Mach number combination considered. It is suggested, however, that the shock detachment distance has a much smaller effect on the incidence calculation than does the stagnation streamline shift and that any reasonable variation will likely be within the accuracy of the method. While other investigators have neglected the detachment distance entirely (e.g., Starken, 1971), the present method uses the above relation as an approximate means to more fully include the effects of suction surface curvature on the length and position of the first captured Mach wave.

As the operating point moves from choke toward stall, the bow shock moves upstream from the blade leading edge and the strong shock region increases, as was shown in Figure 3. The bow shock is pushed forward because there is subsonic flow everywhere behind the passage shock and the downstream pressure information can move upstream around the blade leading edge. Although this mechanism is understood in a broad sense, its effects are difficult to quantify and the shape of the unstarted bow shock can only be predicted with difficulty, even if a Navier-Stokes solver is employed.

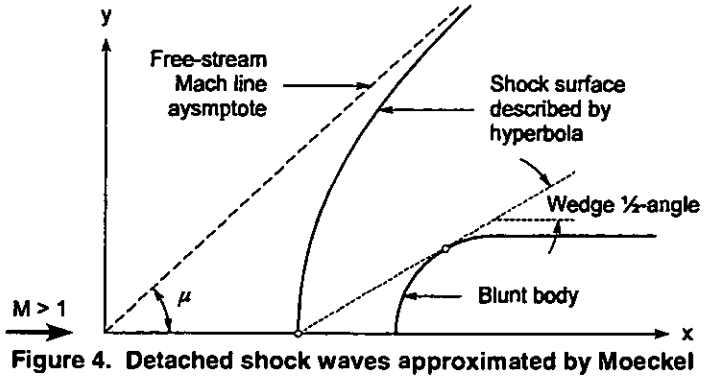

Figure 4. Detached shock waves approximated by Moeckel (1949) method

Because more of the total flow passes through the strong portion of the bow wave during unstarted operation, it is reasonable to anticipate that the loss produced by the bow shock will increase with incidence angle. An approximation of this increased loss has been included in the present model by using an increased "effective leading edge radius" to calculate the bow shock loss for unstarted operation. (The physical coordinates of the blade clearly remain the same, and this increased "effective" leading edge radius is used only in the bow wave loss calculation.)

In the Moeckel (1949) method, the blade leading edge radius is used to calculate the distance between the stagnation streamline and the smooth portion of the blade surface (i.e., the thickness of the forward-most portion of the blade). Because this distance increases by the amount of the stagnation streamline shift during unstarted operation, it is the present authors' opinion that the effective leading edge radius used in the bow shock calculation should be proportional to Δy. Examination of the CFD solutions indicated that the curvature of the sonic line becomes more pronounced after the shock detaches, as represented in Figure 3, suggesting that the effective leading edge radius should increase by somewhat less than Δy.

Recognizing this as an empirical input, the effective leading edge radius used in the bow shock calculation was adjusted to provide satisfactory agreement with the shock loss extracted from CFD for a ***single*** operating point. The comparison was made for the L030-6 cascade with $M_1 = 1.200$ and $\beta_1 = 64.83°$ (near stall), and resulted in the following approximation.

$$LER_{\substack{bow \\ shock \\ loss}} = LER_{blade} + \frac{\Delta y}{2} \tag{9}$$

This relation provided the "effective leading edge radius" used to calculate the bow shock loss for all operating conditions. Clearly, this reduces to the actual blade leading edge radius for the cascade start/unstart point, where $\Delta y = 0$. The Moeckel (1949) method is used to approximate the shape of the detached bow shock using the Mach number along the first captured Mach wave, M_A, and this "effective leading edge radius." The total pressure loss caused by this wave is then calculated from Equation 7.

Before leaving this subject, an important point must be made. While a number of simplifying assumptions have been introduced in the present analysis, Equation 9 represents the only strictly empirical input. The remainder of the present method is obtained by using fundamental fluid mechanics, with certain simplifications and approximations, to analyze the known flow physics.

Passage Shock Position

The passage shock for the cascade start/unstart point is slightly curved and has no supersonic flow downstream. A hyperbola, as described by Moeckel (1949), is used to represent the curved portion of the passage shock between the vertex, B, and the point where the downstream flow is exactly sonic, s, as shown in Figure 5. From the sonic point to the blade suction surface, the passage shock is approximated by a straight line normal to the stagnation streamline at point B. The decrease in total pressure caused by this shock is obtained by numerical integration using 200 points across the passage. The

number of points used in this integration was chosen to allow accurate physical-space location of the shock transition point, s.

The integration steps are determined by equally dividing the axial distance between the blade suction surface coordinate at the first captured Mach wave and at the passage shock intersection point (points A and C in Figure 3). At each point along the blade surface, the Mach number is calculated as a Prandtl-Meyer expansion (or compression) from the upstream condition and a Mach line is extended to the passage shock. For precompression blades, the deceleration produced by the suction surface is assumed to occur isentropically, as a Prandtl-Meyer expansion of opposite sign. As such, this method is applicable to arbitrary airfoil shapes. The variations of upstream Mach number and shock angle are included in the passage shock integration, and the mass-averaged total pressure downstream of the passage shock is given by

$$\frac{\overline{P}_{02}}{P_{0A}} = \frac{\int_B^C \rho V_x \frac{P_{02}}{P_{0A}} dy}{\int_B^C \rho V_x dy} \qquad (10)$$

As the incidence angle increases, the shock detachment distance increases by an amount Δx and the stagnation streamline shifts by an amount Δy. The vertex of the hyperbola is assumed to follow these translations from point B to point B' so that it is always located where the stagnation streamline intersects the bow/passage shock. The curved portion of the shock is reduced by moving the shock transition point forward of the new sonic point, s', by an amount Δx. When the shock transition point reaches the vertex of the hyperbola, the entire shock is approximated as a straight line normal to the stagnation streamline at point B'. As the shock detachment distance continues to increase, the passage shock is approximated as a straight line, normal to the stagnation streamline, from point B'' to point C''. The total pressure ratio across the passage shock is given by Equation 10.

Model Predictions

The total pressure loss coefficients for unstarted operation of the L030-6 cascade with an inlet Mach number of 1.20 are shown in Figure 6. As stated previously, the CFD solutions were obtained with no sidewall variation ($AVDR \equiv 1$). The points labeled "Experiment" were obtained from Schreiber (1980), while the points labeled "Fit to Data" were obtained from the shock loss curves fit by Schreiber (1987) to his measurements (i.e., by evaluating the dashed curve labeled ω_{shock} in Figure 2). The CFD solutions are shown to provide fairly accurate prediction of the overall loss for the entire operating range of this

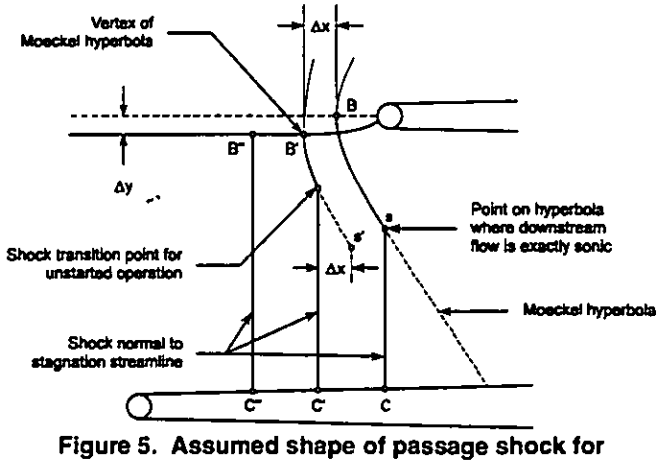

Figure 5. Assumed shape of passage shock for unstarted operation

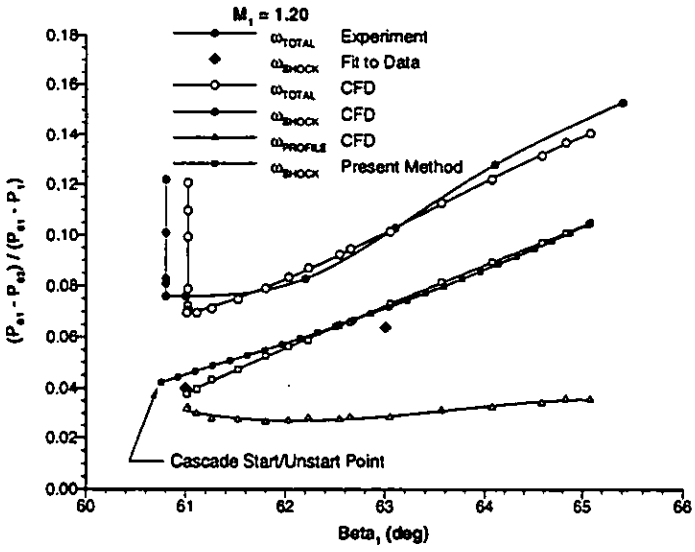

Figure 6. Loss coefficient comparison for unstarted operation of the L030-6 cascade with M_1 = 1.20

cascade. This suggests that the RVCQ3D Navier-Stokes analysis tool can be used to supplement the available measurements and that the differences between these predictions and the measurements are likely to be small.

The most significant point made by this figure is the dramatic increase in shock loss as the inlet flow angle increases. This is shown clearly by the data, by the CFD solutions, and by the model predictions. The viscous profile loss predicted by the CFD is seen to be nearly constant over the entire unstarted operating range, with a variation of less than 0.010 between the minimum and maximum unstarted loss coefficients. The actual viscous loss is likely to be slightly larger near stall than indicated by the CFD solutions, which show a suction surface boundary layer separation downstream of the passage shock. It is the authors' opinion, however, that the actual variation of viscous loss between stall and choke will still be significantly smaller than the variation of shock loss over the same operating range.

To understand the significance of the level of accuracy demonstrated in this figure, it is helpful to consider the recent ASME turbomachinery CFD "blind" test case (Strazisar and Denton, 1995). To obtain an accuracy of ±1-2% in pressure rise and of ±1% in efficiency in that test case, the predicted total pressure loss coefficient must be accurate within 0.010 (Dunham, 1995). Although the viscous loss has not been addressed in the present method, the accuracy of the predicted shock loss coefficients in Figure 6 clearly falls within this range.

Figure 7 shows the total pressure loss coefficients for unstarted operation of the L030-6 cascade with an inlet Mach number of 1.12. As before, there is a significant increase in shock loss with incidence, the viscous profile loss is nearly constant (0.009 difference between maximum and minimum), and the present shock loss model predictions are within the desired 0.010 accuracy.

To illustrate another trend shown in the 2 previous figures, the shock loss and viscous profile loss coefficients obtained from the CFD solutions for the L030-6 cascade are plotted in Figure 8. The shock loss is clearly much more sensitive to Mach number than is the profile loss. For the Mach number range considered, the increase in shock loss with Mach number is 3 to 18 times as large as the increase in profile loss (assuming β_1 is held fixed). This observation supports Schreiber's (1987) conclusion that the increase in total pressure loss that occurs with increasing Mach number is predominantly caused by an increase in shock loss.

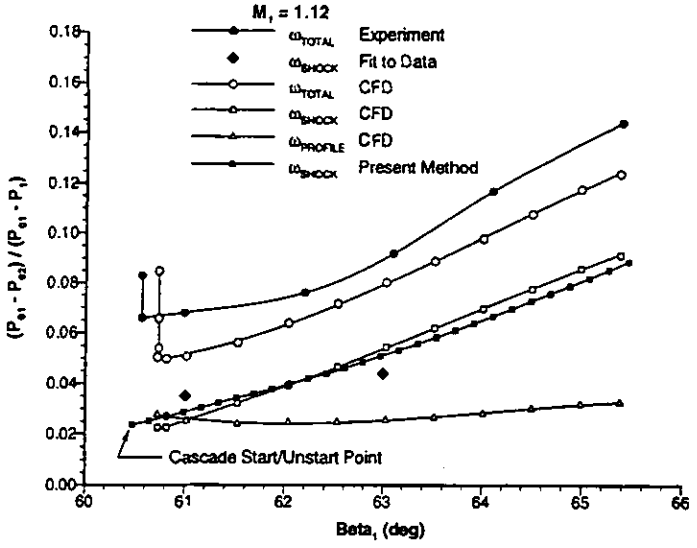

Figure 7. Loss coefficient comparison for unstarted operation of the L030-6 cascade with M_1 = 1.12

The present shock loss predictions have shown good agreement with both the experimental measurements and the CFD results for unstarted operation of the L030-6 cascade over the range of inlet Mach numbers considered. Agreement with this data set alone, however, cannot be considered as proof of the general applicability of the method because the empirical constant in the bow shock model was adjusted to match the performance of this cascade (although at a single near-stall condition). To further establish the validity of the present shock loss model, the performance of the L030-4 cascade was predicted. Because there are significant differences in profile shape and blade angles between these 2 configurations, and because empirical information from the L030-4 cascade test was not used to develop the model, this is a true prediction that can be used to evaluate the accuracy of the present method.

The total pressure loss coefficients for unstarted operation of the L030-4 cascade with an inlet Mach number of 1.10 are shown in Figure 9. The CFD solutions show a strong increase in shock loss with increasing inlet flow angle, as was shown for the L030-6 solutions,

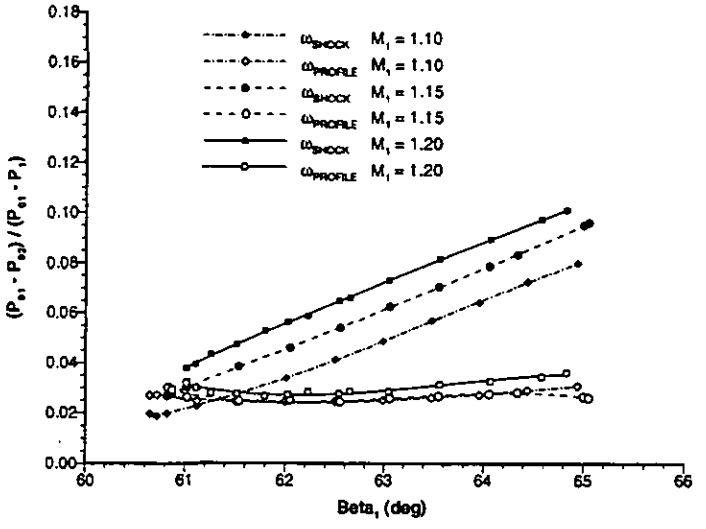

Figure 8. Comparison of the shock loss and viscous profile loss coefficients obtained from the CFD solutions for unstarted operation of the L030-6 cascade

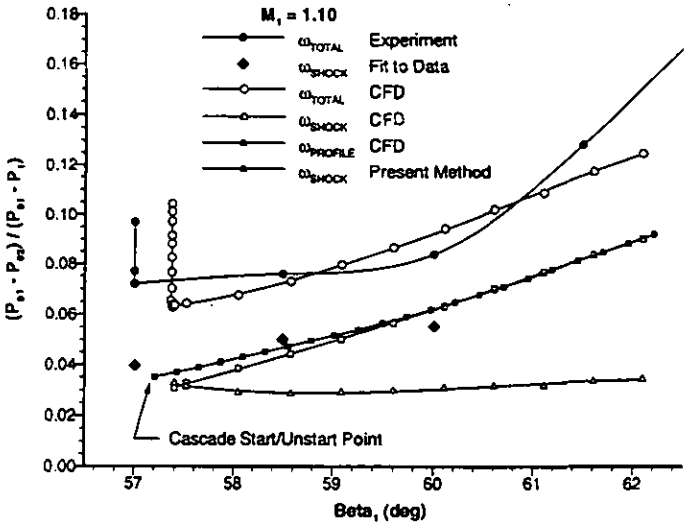

Figure 9. Loss coefficient comparison for unstarted operation of the L030-4 cascade with M_1 = 1.10

while the viscous profile loss is nearly constant (0.007 difference between maximum and minimum). As in the previous figures, the desired accuracy of 0.010 between the present shock loss model predictions and the available validation tools has been demonstrated for the L030-4 cascade.

Discussion

The present prediction method considers the total pressure deficit that is produced by the detached bow waves that stand ahead of the cascade. While Starken, et al. (1984) suggested this effect be included in the continuity equation for the minimum-incidence calculation, it has not been included in previously published shock loss models. To demonstrate the significance of the bow shock loss as a fraction of the present shock loss prediction, the following bow shock loss coefficient is defined.

$$\omega_{bow} = \frac{P_{01} - P_{0A}}{P_{01} - P_1} \tag{11}$$

where P_{0A}/P_{01} is the total pressure reduction caused by the detached bow shock (obtained from Equation 7). A passage shock loss coefficient is then defined as the difference between the predicted shock loss coefficient and the bow shock loss coefficient.

$$\omega_{passage} = \omega_{shock} - \omega_{bow} \tag{12}$$

Figure 10 identifies the bow-shock and passage-shock loss components of the present prediction method for unstarted operation of the L030-6 cascade with inlet Mach number of 1.20[1]. The trends shown in this figure are representative of the other operating points considered for both the L030-6 and L030-4 cascades. The measured shock loss coefficients and the values obtained from CFD are included for comparison, but the overall loss and the viscous loss obtained from CFD are omitted from this figure for clarity.

The bow shock loss is shown to be small at the cascade start/unstart point, with a value of 0.004. This is consistent with observations of the CFD solutions which indicate that the rotational effects of the bow

[1] Symbols are omitted from the bow shock and passage shock loss curves in Figure 10 to indicate that these are only a *portion* of the present shock loss prediction method and should not be considered separately.

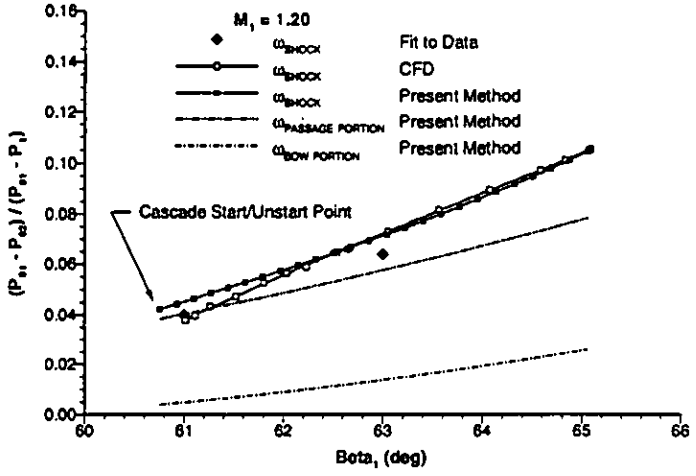

Figure 10. Identification of loss attributed to passage shock and to bow wave for unstarted operation of the L030-6 cascade with $M_1 = 1.20$

shock are small during started operation and, except for a small region near the blade surface, that the entrance-region characteristics are nearly straight. The bow shock loss increases significantly with incidence, and is about 0.025 near stall. This is again consistent with the CFD solutions, which indicate that the strong portion of the bow wave extends farther from the blade as incidence increases.

The present bow wave calculation has significant effects on the predicted shock loss coefficients. While the effect of this bow shock is small at the start/unstart point, it is clearly important as incidence increases. This suggests that the bow shock produces a significant fraction of the shock loss during unstarted operation, and that this mechanism must be included in an off-design performance model. Another effect is that inclusion of the bow shock loss in the continuity equation results in a slightly higher Mach number along the first captured Mach wave. This higher Mach number then produces passage shock loss coefficient that is between 0.002 and 0.010 larger than if the bow wave loss were neglected.

Comparison with Previously Published Models

The curved portion of the unstarted passage shock is small and the entire passage shock can be reasonably approximated as a normal shock, as suggested by Miller, et al. (1961) and by Wennerstrom and Puterbaugh (1984). Both of these models calculated the Mach number

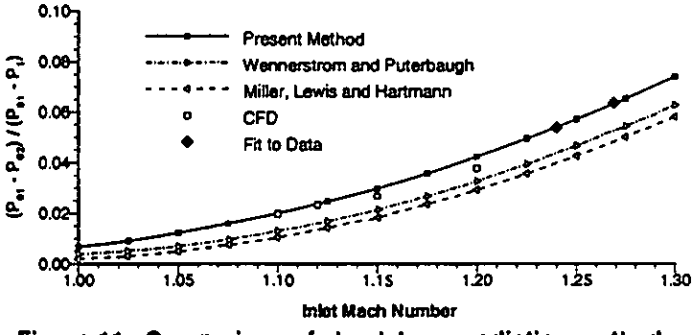

Figure 11. Comparison of shock loss prediction methods for the L030-6 cascade start/unstart point as a function of inlet Mach number

at the suction surface shock impingement point as a Prandtl-Meyer expansion from the upstream condition, as has been done in the present method. In the previous models, however, the Mach number on the pressure side of the passage (the blade leading edge) was assumed to be the upstream value rather than the value along the first captured Mach wave. Because the flow undergoes a Prandtl-Meyer expansion around the blade leading edge, the Mach number along the first captured Mach wave is generally higher than the upstream value and the above methods will slightly under-predict the loss.

In the present investigation, both the upstream Mach number and the shock obliqueness angle are determined by extending a Mach line from the suction surface to the passage shock at 200 locations. This approach allows a more accurate inclusion of the nonlinear effects of Mach number and shock angle on total pressure loss than do the previously published methods. The improved agreement obtained from the present method is shown in Figure 11 for the start/unstart point of the L030-6 cascade operated over a range of inlet Mach numbers. Comparison with the Miller, et al. (1961) and the Wennerstrom and Puterbaugh (1984) shock loss models over a range of inlet flow angles is not possible because the previously published methods are applicable only at the minimum overall loss point (i.e., the cascade start/unstart point).

Conclusions

A physics-based model has been presented for the prediction of shock losses over the entire supersonic operating range of compressor cascades with arbitrary airfoils. This model has been shown to accurately capture the shock loss trends and magnitudes for unstarted operation of both the L030-4 and L030-6 cascades for the range of inlet Mach numbers considered, and the following conclusions can be drawn from this investigation.

- The dramatic increase in overall loss with increasing inlet flow angle is primarily the result of increased shock loss. For a given Mach number, the viscous profile loss is nearly constant over the entire unstarted operating range of the cascade, unless a shock-induced boundary layer separation occurs near stall.
- Much of the increased total pressure loss that occurs with increasing incidence is caused by the detached bow shock.
- Shock loss is much more sensitive to inlet Mach number than is viscous profile loss.

Acknowledgments

The authors wish to thank Rod Chima of the NASA Lewis Research Center for providing the quasi-3-D Navier-Stokes solver used in the present investigation, for explanation of the appropriate boundary conditions, and for general advice on interpretation of the solutions. Gratitude is also expressed to Dan Tweedt of NASA Lewis for some fairly lengthy discussions on the difficult nature of supersonic compressor cascade testing and the limitations of these test results. Heinz-Adolf Schreiber of the DLR has provided the measured blade coordinates from the L030 cascade tests. While these are available in the published literature, the electronic transfer of these coordinates avoided the tedious and error-prone process of typing them in by hand.

In addition, the authors would like to thank the members of the Compressor Aero Research Lab team who have contributed to the present effort. Finally the authors thank the management at Wright Laboratory and Air Force Office of Scientific Research for their continued support of our research efforts.

References

Balzer, R. L., 1971, "A Method of Predicting Compressor Cascade Total Pressure Losses When the Inlet Relative Mach Number is Greater than Unity," ASME *Journal of Engineering for Power*, Vol. 93, No. 1, pp. 119-125.

Casey, M. V., 1994a, "Computational Methods For Preliminary Design And Geometry Definition In Turbomachinery," AGARD LS-195, Paper 1.

Casey, M. V., 1994b, "Industrial Use of CFD in the Design of Turbomachinery," AGARD LS-195, Paper 6.

Chima, R. V., 1987, "Explicit Multigrid Algorithm for Quasi-Three-Dimensional Viscous Flows in Turbomachinery," AIAA *Journal of Propulsion and Power*, Vol. 3, No. 5, pp. 397-405.

Chima, R. V., Turkel, E., and Schaffer, S., 1987, "Comparison of Three Explicit Multigrid Methods for the Euler and Navier-Stokes Equations," NASA TM-88878.

Denton, J. D., 1993, "Loss Mechanisms in Turbomachines," ASME *Journal of Turbomachinery*, Vol. 115, No. 4, pp. 621-656.

Denton, J. D., 1994, "Designing in Three Dimensions," AGARD LS-195, Paper 3.

Dunham, J., 1995, "Aerodynamic Losses in Turbomachines," AGARD CP-571, Keynote Address.

Dunker, R. J., Strinning, P. E., Weyer, H. B., 1978, "Experimental Study of the Flow Field within a Transonic Axial Compressor Rotor by Laser Velocimetry and Comparison with Through-Flow Calculations," Transactions of the ASME , Series A, Vol. 100, p.279.

Dunker, R. J, and Hungenberg, H. G., 1980, "Transonic Axial Compressor Using Laser Anemometry and Unsteady Pressure Measurements," AIAA Journal, Vol. 18, pp. 973-979.

Freeman, C., and Cumpsty, N. A., 1992, "A Method for the Prediction of Supersonic Compressor Blade Performance," AIAA *Journal of Propulsion and* Power, Vol. 8, No. 1, pp. 199-208.

Jenions, I. K., 1994, "The Role of CFD in the Design Process," AGARD LS-195, Paper 8.

Kantrowitz, A., 1950, "The Supersonic Axial-Flow Compressor," NACA Report 974.

Klapproth, J. F., 1950, "Approximate Relative-Total-Pressure Losses of an Infinite Cascade of Supersonic Blades With Finite Leading-Edge Thickness," NACA RM E9L21.

Koch, C. C., 1995, "Loss Mechanisms and Unsteady Flows in Turbomachines," AGARD CP-571, Technical Evaluation Report.

Koch, C. C., and Smith, L. H., 1976, "Loss Sources and Magnitudes in Axial-Flow Compressors," ASME *Journal of Engineering for Power*, Vol. 98, pp. 411-424.

Levine, P., 1956, "The Two Dimensional Inflow Conditions for a Supersonic Compressor With Curved Blades," Wright Air Development Center TR 55-387.

Lichtfuß, H. -J., and Starken, H., 1974, "Supersonic Cascade Flow," DFVLR Sonderdruck Nummer 376, reprinted in *Progress in Aerospace Science*, Pergammon Press Ltd., Volume 15.

Lieblein, S., 1954, "Review of High-Performance Axial-Flow Compressor Blade Element Theory," NACA RM E53L22.

Miller, G. R., Lewis, G. W., Hartmann, M. J., 1961, "Shock Losses in Transonic Compressor Blade Rows," ASME *Journal of Engineering for Power*, Vol. 83, pp. 235-242.

Moeckel, W. E., 1949, "Approximate Method for Predicting Form and Location of Detached Shock Waves Ahead of Plane or Axially Symmetric Bodies," NACA TN 1921.

Novak, R. A., 1967, "Streamline Curvature Computing Procedures for Fluid-Flow Problems," ASME *Journal of Engineering for Power*, Vol. 93, pp. 478-490.

Schreiber, H.-A., 1980, "Untersuchungen am Verdichtergitter L030-6 im transsonischen Machzahlbereich von M_1=0,8 bis 1,24 - Schaufelschnitt des Transsonikverdichter-Laufrades 030 bei 68% Schaufelhöhe" DFVLR IB 352-80/2.

Schreiber, H.-A., 1981, "Experimentelle Untersuchung des Verdichtergitters L030-4 mit Variation des axialen Massenstromdichteverhältnisses im transsonischen Machzahlbereich," DFVLR IB 325l4l1981.

Schreiber, H.-A., 1987, "Experimental Investigations on Shock Losses of Transonic and Supersonic Compressor Cascades," AGARD CP-401, Paper 11.

Schreiber, H.-A. and Starken, H., 1981, "Evaluation of Blade Element Performance of Compressor Rotor Blade Cascades in Transonic & Low Supersonic Flow Range," Fifth International Symposium on Airbreathing Engines, Paper 67, Bangalore, India.

Schreiber, H.-A., and Tweedt, D. L., 1987, "Experimental Investigation and Analysis of the Supersonic Compressor Cascade ARL-2DPC," DFVLR IB-325-02-87.

Sorenson, R. L., 1981, "A Computer Program to Generate Two-Dimensional Grids About Airfoils and Other Shapes by the Use of Poisson's Equation," NASA TM-81198.

Starken, H., 1971, "Untersuchung der Strömung in ebenen Überschallverzögerungsgittern (Investigation of the Flow in Planar Supersonic Compressor Cascades)," DFVLR FB 71-99.

Starken, H., Zhong, Y., and Schreiber, H.-A., 1984, "Mass Flow Limitation of Supersonic Blade Rows Due to Leading Edge Blockage," ASME paper 84-GT-233.

Strazisar, A. J., and Denton, J. D., 1995, "CFD Code Assessment in Turbomachinery - A Progress Report," IGTI *Global Gas Turbine News*.

Vuillez, C., and Petot, B., 1994, "New Methods, New Methodology: Advanced CFD in the SNECMA Turbomachinery Design Process," AGARD LS-195, Paper 7.

Wennerstrom, A. J., and Puterbaugh, S. L., 1984, "A Three-Dimensional Model for the Prediction of Shock Losses in Compressor Blade Rows," ASME *Journal of Engineering for Gas Turbines and Power*, Vol. 106, No. 2 pp. 295-299.